Intersection Point-Based Analysis of Neural Balance Control Strategies by Parkinson's Patients during Quiet Stance

Gayatri Sreenivasan, Chunchu Zhu, and Jingang Yi

Abstract— **This study employs intersection point height frequency analysis to quantitatively assess the balance control strategies used by individuals with Parkinson's disease (PD) during quiet stance. The changes in balance strategy are quantified using a triple inverted pendulum human model with a linear quadratic regulator as the neural balance controller. By considering both translational and angular body accelerations, we extract intersection point frequency curves that contain crucial information about the neuromuscular balance strategy of the PD patients. To contextualize our findings, we compare the observed frequency behavior with previous studies examining quiet stance in individuals without PD. This comprehensive investigation furnishes valuable insights into the disparities between the balance strategies of the PD patients and the healthy counterparts, shedding light on the influence of PD on balance control dynamics. The findings hold promising potential for applications in PD diagnostics and the development of robotic assistive devices for PD patient rehabilitation.**

I. Introduction

Parkinson's disease (PD) is an idiopathic chronic neurodegenerative disorder [1], [2]. The progressive PD condition manifests in various motor symptoms, including tremors, rigidity, bradykinesia (slowness of movement), and postural instability, along with a range of non-motor symptoms [3]. Currently, there is no cure for PD, but medications like levodopa help patients manage their symptoms. PD diagnosis relies on observing motor symptoms and excluding other possible disorders. An early and accurate diagnosis is crucial to ensure patients receive timely medical care and proactive symptom management. Earlier physiotherapy can help reveal how the patient has been affected by the disease [4]. A thorough investigation of motor behavior in PD patients is essential to identify potential gait-based indicators of PD.

Recent studies have investigated robotic assistive devices in PD neuromuscular rehabilitations and balance enhancements [5]–[9]. However, developing effective robotic interventions requires a holistic understanding of PD patients' neural balance mechanisms to improve their movement quality. Quiet stance becomes intricate in PD patients due to limited insights into the factors contributing to destabilization and the strategies employed to counteract instability. Studies have explored postural instability in PD [10], employing various analytical metrics. Additionally, efforts have been made to construct neuromechanical models aimed at quantifying the PD gait abnormalities [11], [12].

This study complements existing research by investigating gait frequencies of PD patients using the intersection point (IP) height concept [13]. A double-inverted pendulum model was introduced in [14] to analyze the findings of [13]. Recent studies highlight the non-trivial aspect of knee movements in balance strategies during quiet stance [15], [16]. To account for knee excursions, the double-inverted pendulum model was expanded into a triple-inverted pendulum (TIP) model in [17]. IP height analysis has been employed to perform gait frequency analysis in balancing strategies in walking [18], robotic control [19], quiet standing [13] and prostheses evaluation [17], [20]. This method offers a unique advantage over traditional balance assessments like center of pressure (COP) or center of mass (COM) by providing insights into both the translational and rotational body accelerations [21].

This work analyzes the neural balance strategy and behavior of PD patients under various conditions and diagnostic categories using the IP analysis. By examining specific PD groups, we gain a comprehensive understanding of the dynamic nature of balance changes in the PD patient population. The study employs a linear quadratic regulator (LQR)-controlled TIP model to mimic human quiet stance dynamics. The LQR represents the human neural controller to quantify the specific parameters that define the balance strategy. A novel contribution is the introduction of the IP frequency curve as a quantifiable PD indicator, offering diagnostic value and insights into PD affected neural balance control mechanisms. The findings can be further extended to develop effective and personalized robotic assistive devices and controllers that would improve the mobility for individuals living with PD.

This paper is organized as follows. An overview of the neural balance control model and IP analysis method are given in Section II. Section III details patient data and the model data and the results. The implications of the observations are discussed in Section IV. Section V summarizes the concluding remarks.

II. Method

In this section, we first present the LQR-controlled TIP model. Then the IP concept for human postural balance in quiet stance is reviewed. Finally, the IP height frequency method is presented.

This work was supported in part by US NSF awards CMMI-2222880 and DGE-2021628.

G. Sreenivasan is with the Department of Electrical and Computer Engineering, Rutgers University, Piscataway, NJ 08854 USA (email: gs912@scarletmail.rutgers.edu).

C. Zhu and J. Yi are with the Department of Mechanical and Aerospace Engineering, Rutgers University, Piscataway, NJ 08854 USA (email: chunchu.zhu@rutgers.edu, jgyi@rutgers.edu).

A. Neural Balance Control Model

The neural balance control model comprises of the TIP biomechanical model and the LQR controller. As shown in Fig. 1(a), the TIP model assumes that human body motion occurs only in the sagittal plane and that the human is on a rigid surface [17]. The TIP model includes the lower link (shank), middle link (thigh) and upper link (head, arms and torso). The mass, joint angle with vertical line, length, COM position, and moment of inertia of the lower, middle and upper links are denoted by m_i, θ_i, l_i, l_{ci}, and I_i, $i = 1, 2, 3$, respectively. Table I lists the parameters and their corresponding values that are used in this study.

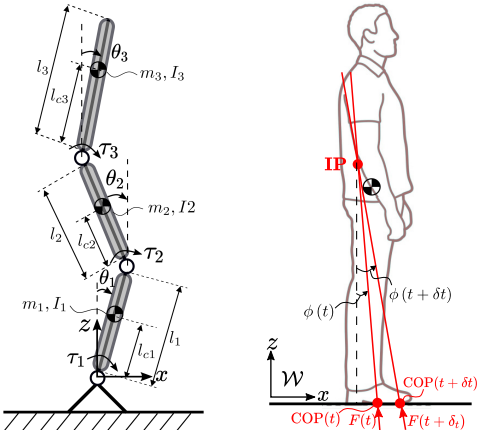

(a) (b)

Fig. 1. (a) Triple inverted pendulum model to represent a human at quiet stance. (b) Visualization of the IP.

TABLE I

MODEL PARAMETERS FOR THE TIP MODEL

Parameter	Link 1	Link 2	Link 3
m_i (kg)	6.5	16.5	53
l_i (m)	0.415	0.413	0.793
l_{ci} (m)	0.24	0.255	0.265
I_i (kgm^2)	0.1	0.3	3

Similar to [17], denoting $\boldsymbol{\theta} = [\theta_1 \ \theta_2 \ \theta_3]^T$, the equation of motion for the TIP is written as

$$\boldsymbol{M}(\boldsymbol{\theta})\ddot{\boldsymbol{\theta}} + \boldsymbol{C}(\boldsymbol{\theta}, \dot{\boldsymbol{\theta}})\dot{\boldsymbol{\theta}} + \boldsymbol{G}(\boldsymbol{\theta}) = \boldsymbol{\tau} \tag{1}$$

where $\boldsymbol{M}(\boldsymbol{\theta})$, $\boldsymbol{C}(\boldsymbol{\theta}, \dot{\boldsymbol{\theta}})$, and $\boldsymbol{G}(\boldsymbol{\theta})$ are the inertia, Coriolis, and gravitational matrices, respectively. The joint torques $\boldsymbol{\tau}$ is given as

$$\boldsymbol{\tau} = \boldsymbol{\tau}_{st} + \boldsymbol{\omega},$$

where $\boldsymbol{\tau}_{st} = [\tau_1 \ \tau_2 \ \tau_3]$ is the stabilizing torque vector and $\boldsymbol{\omega}$ is the joint perturbations that are represented by an uncorrelated white Gaussian noise vector with zero mean and variance $\boldsymbol{\sigma} = \text{diag}(\sigma_1^2, \sigma_2^2, \sigma_3^2)$. The GRFs are computed using the total body mass ($m_{tot} = m_1 + m_2 + m_3$) and the COM accelerations in the horizontal (a_x) and vertical (a_z) directions, that is,

$$F_x = m_{tot} a_x, \ F_z = m_{tot}(a_z + g).$$

The anterior-posterior (AP) COP position is computed as

$$\text{COP}_x = \tau_1 / F_z.$$

Let $\boldsymbol{x} = [\boldsymbol{\theta}^T \ \dot{\boldsymbol{\theta}}^T]^T$ denote the state variable. To model the neural motor stabilization as an LQR controller, we linearize (1) around the upright balancing position, denoted as $\boldsymbol{x}^* = \boldsymbol{0}$ and $\boldsymbol{\tau}^* = \boldsymbol{0}$. Using the small angle approximation, the linear state space model is as follows.

$$\dot{\bar{\boldsymbol{x}}} = \boldsymbol{A}_{\text{lin}}\bar{\boldsymbol{x}} + \boldsymbol{B}_{\text{lin}}(\bar{\boldsymbol{\tau}} + \boldsymbol{\omega})|_{\bar{\boldsymbol{x}}=\boldsymbol{x}-\boldsymbol{x}^*, \bar{\boldsymbol{\tau}}=\boldsymbol{\tau}-\boldsymbol{\tau}^*}, \tag{2}$$

where $\boldsymbol{A}_{\text{lin}}$ and $\boldsymbol{B}_{\text{lin}}$ represent the linearized state space matrices. For detail information about these matrices, readers can refer to [17]. We introduce positive definite symmetric matrices $\boldsymbol{Q}$ and $\boldsymbol{R}$ to penalize the state and control inputs in the LQR cost function

$$J = \int_0^\infty \left[\bar{\boldsymbol{x}}^T(t)\boldsymbol{Q}\bar{\boldsymbol{x}}(t) + \bar{\boldsymbol{\tau}}^T(t)\boldsymbol{R}\bar{\boldsymbol{\tau}}(t)\right] dt. \tag{3}$$

By minimizing (3), we obtain the gain matrix $\boldsymbol{K}_{\text{st}}$ and the stabilizing torques are computed as

$$\boldsymbol{\tau}_{st} = -\boldsymbol{K}_{st}\boldsymbol{x}. \tag{4}$$

The LQR controller serves as the neural controller and ensures the stability of the closed-loop system if the $(\boldsymbol{A}_{\text{lin}}, \boldsymbol{B}_{\text{lin}})$ pair is controllable. The matrix $\boldsymbol{Q} = \boldsymbol{I}_6$ (identity matrix) is used to uniformly penalize deviations in each state. Matrix $\boldsymbol{R}$ is defined as

$$\boldsymbol{R} = \alpha \ \text{diag}(\beta_1, \beta_2, \beta_3),$$

where α represents the relative cost between the state deviation and control effort, and $\boldsymbol{\beta} = [\beta_1 \ \beta_2 \ \beta_3]^T$ represents the relative magnitude of joint effort at the ankle, knee and hip joints, respectively. These parameters, along with $\boldsymbol{\sigma}$, constitute the variable set that characterizes the control strategy.

B. Intersection Point Height

The IP is defined as the point at which the ground reaction force (GRF) vectors intersect at consecutive time instants; see Fig. 1(b). The GRF direction ($\phi(t)$) is approximated as the absolute value of the reciprocal of the horizontal (F_x) and vertical (F_z) components, that is,

$$\phi(t) \approx \left|\frac{F_x}{F_z}\right|. \tag{5}$$

The human subject's height is measured to approximate the COM. Only the AP component of the COP is considered for IP height computation.

While there is no apparent relation between the unfiltered COP and $\phi(t)$, the signals are known to be correlated for frequencies greater than 0.4 Hz [13]. In order to unveil their underlying relationship, the signals are initially processed using a Hann window. A zero-lag, 2nd order Butterworth filter is used to parse the signals into frequency bands of 0.2 Hz width to finally reveal an approximately linear trace. The reciprocal of the slope of the trace is defined as the

height of the IP for the band considered. This process is repeated to get 38 non-overlapping bands with frequencies centered from 0.5 Hz to 7.9 Hz at 0.2 Hz increments. The resultant IP height frequency curve is used for analysis.

Fig. 2 shows the IP height varying with frequency for a healthy subject during quiet stance. The IP height is plotted as the normalized value with respect to the COM height. Hence, one in the IP curve figure indicates the COM height. It is widely acknowledged that the quiet stance IP frequency curves of healthy individuals adhere to three distinct characteristic patterns [13]: (1) the IP is located above the COM height at lower frequencies, (2) the IP height decays as frequency increases, and (3) the IP height reaches an asymptote below COM height at high frequencies. The crossover frequency (CF) and the high-frequency asymptote (HFA) are two pivotal metrics used to rigorously assess the behavior of the IP curves. The CF marks the precise frequency at which the IP curve dips below the COM, while the HFA characterizes the IP curve's behavior at high frequencies. These metrics are crucial for analyzing IP curve dynamics.

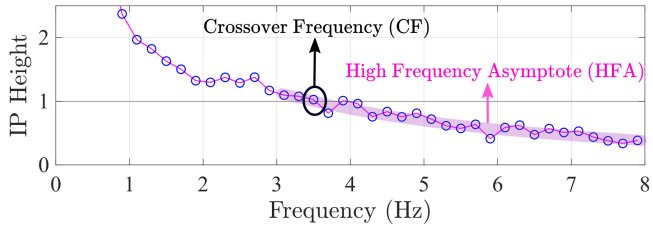

Fig. 2. A typical IP curve of a healthy subject during quiet stance.

C. Statistical Analysis Method

Fig. 3 outlines the overall procedure for IP-based data analysis. The GRF and COP data were first derived from the experimental and simulation data. Frequency curves were then extracted, followed by statistical analysis for for the datasets of each subject group. The characteristic of the IP curve was assessed through the quantification of three key model parameters, namely, α, $\boldsymbol{\beta}$ and $\boldsymbol{\sigma}$. To enable robust statistical analysis of the dependency of the IP height on frequency, simulation studies were conducted using the LQR-controlled TIP model. To collect enough data for analysis, 30 trials were conducted for each parameter set and each trial lasted 50 s at a sampling rate of 100 Hz. The parameter sets include α, $\boldsymbol{\beta}$ and $\boldsymbol{\sigma}$. The physiological significance of these parameters was elaborated in [14] as follows: (1) $\boldsymbol{\alpha}$ characterizes the control effort employed to attain stability, (2) $\boldsymbol{\beta}$ denotes the relative penalty for joint control, and (3) $\boldsymbol{\sigma}$ signifies neuromuscular noise at each joint.

III. Experiments and Results

In this section, we first introduce the dataset of PD patients used in our study. Subsequently, we present the results of IP frequency curve extraction, followed by a detailed analysis of our findings and relevant observations.

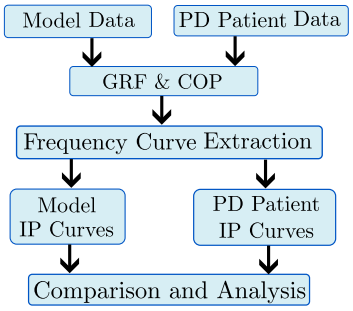

Fig. 3. Pipeline of the IP height analysis.

A. PD Patients Dataset

We conducted an extensive statistical analysis using a publicly available dataset that was published in [22]. This dataset contains valuable biomechanical data acquired during experimental trials involving PD patients' quiet stance. Specifically, it provides GRFs and COP data in the AP direction, which are essential for conducting IP height frequency analysis. The experimental protocol had the subjects to perform quiet standing under various testing conditions including: (i) standing on a rigid surface (RS) or unstable surface (US), (ii) having their eyes open (EO) or eyes closed (EC) and (iii) being on medication (ON) or off medication (OFF).

The patient trials were first sorted into 8 cases of interest (COI) as listed in Table II. In addition to the 8 COIs that arose from the changing test protocol, 4 other groups of interest (GOI) were formed from the subjects with varied PD diagnoses. This meticulous categorization allows for a comprehensive analysis of the dataset, enhancing the ability to draw meaningful conclusions. Table III lists the detailed GOI data information. We considered essential PD phenotypes, specifically, tremor-dominant (TD) and postural instability and gait difficulty (PIGD), as the GOIs. The PIGD subtype manifests symptoms like bradykinesia, rigidity during movement, and a notably rapid disease progression. Conversely, the TD subtype is characterized by a resting tremor, normal gait, and a gradual disease progression. Notably, PIGD-diagnosed patients tend to experience significantly greater intellectual, motor, and occupational impairment than TD patients. Moreover, they are at a higher risk of developing conditions such as dementia, depression, and apathy, as noted in [23]. Furthermore, two other GOIs were formed based on the presence or absence of freezing of gait (FoG), distinguished as freezers and non-freezers. The comprehensive categorization explores various aspects of PD and its implications on balance and gait dynamics.

This dataset reports data from 32 patients, with 3 trials conducted for each of the 8 COIs for every patient, amounting to a total of 767 trials (32 patients $\times$ 8 cases per patient $\times$ 3 trials per case, with one missing trial). A single IP frequency curve was computed for each trial, as explained in Section II-B. Subsequently, we generated a mean IP curve by aggregating data from all trials corresponding to a specific

TABLE II
CASES OF INTEREST

S	COI	IP Curve Linear Fit
1	EO+RS+OFF	$y = -0.01685x + 0.8013$
2	EO+RS+ON	$y = -0.01058x + 0.772$
3	EO+US+OFF	$y = -0.007991x + 0.7679$
4	EO+US+ON	$y = -0.001201x + 0.8079$
5	EC+RS+OFF	$y = 0.000614x + 0.706$
6	EC+RS+ON	$y = 0.008483x + 0.7158$
7	EC+US+OFF	$y = 0.02152x + 0.7341$
8	EC+US+ON	$y = -0.02027x + 0.8597$

TABLE III
GROUPS OF INTEREST

S	GOI	COI	IP Curve Linear Fit
1	PIGD	EO+RS+OFF	$y = -0.02305x + 0.8606$
2	PIGD	EO+RS+ON	$y = -0.03237x + 0.9131$
3	PIGD	EO+US+OFF	$y = -0.003184x + 0.7444$
4	PIGD	EO+US+ON	$y = 0.04575x + 0.6329$
5	PIGD	EC+RS+OFF	$y = -0.00009x + 0.7305$
6	PIGD	EC+RS+ON	$y = -0.01172x + 0.8153$
7	PIGD	EC+US+OFF	$y = 0.08529x + 0.5518$
8	PIGD	EC+US+ON	$y = -0.01529x + 0.8124$
9	TD	EO+RS+OFF	$y = -0.01379x + 0.7693$
10	TD	EO+RS+ON	$y = 0.002647x + 0.688$
11	TD	EO+US+OFF	$y = -0.01113x + 0.7847$
12	TD	EO+US+ON	$y = -0.0298x + 0.9179$
13	TD	EC+RS+OFF	$y = 0.001244x + 0.6911$
14	TD	EC+RS+ON	$y = 0.02184x + 0.6541$
15	TD	EC+US+OFF	$y = -0.00969x + 0.7883$
16	TD	EC+US+ON	$y = -0.02594x + 0.897$
17	Freezers	EO+RS+OFF	$y = -0.02049x + 0.848$
18	Freezers	EO+RS+ON	$y = 0.002115x + 0.7143$
19	Freezers	EO+US+OFF	$y = -0.002411x + 0.7586$
20	Freezers	EO+US+ON	$y = 0.03745x + 0.6795$
21	Freezers	EC+RS+OFF	$y = -0.0004105x + 0.7295$
22	Freezers	EC+RS+ON	$y = 0.01392x + 0.7701$
23	Freezers	EC+US+OFF	$y = -0.01328x + 0.8394$
24	Freezers	EC+US+ON	$y = -0.02296x + 0.8918$
25	Non-Freezers	EO+RS+OFF	$y = -0.01436x + 0.7694$
26	Non-Freezers	EO+RS+ON	$y = -0.01927x + 0.8114$
27	Non-Freezers	EO+US+OFF	$y = -0.01162x + 0.7721$
28	Non-Freezers	EO+US+ON	$y = -0.02765x + 0.8956$
29	Non-Freezers	EC+RS+OFF	$y = 0.001315x + 0.6907$
30	Non-Freezers	EC+RS+ON	$y = 0.004763x + 0.6787$
31	Non-Freezers	EC+US+OFF	$y = 0.04532x + 0.662$
32	Non-Freezers	EC+US+ON	$y = -0.01848x + 0.8383$

combination of GOI and COI.

B. Experimental IP Height Curve Analysis

Fig. 4 illustrates a comparison between an IP curve of a healthy subject and the mean IP curve derived from all COIs of PD patients. The stark difference between the two curves arises from the PD patient's behavior, which deviates from the three well-established patterns governing IP curves in healthy subjects. While prior IP-based investigations (e.g., [17]) relied on exponential-fitted IP curves for quantitative analysis, it is evident that this approach becomes inadequate for PD patients. Consequently, we adopt linear fitting to compare the IP curves of PD patients, which exhibit a relatively flat profile interspersed with sporadic spikes of varying amplitudes.

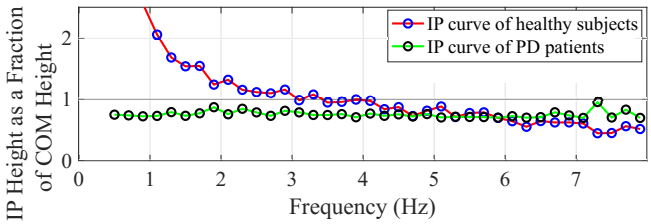

Fig. 4. Comparison of IP curve between healthy subjects and PD patients.

Fig. 5(a) shows the mean IP curves for the COIs. The highest spikes at high frequencies are generated by the "EC+US+OFF" case, followed by the "EO+US+ON" and "EC+RS+ON" cases. The highest spike at lower frequencies (2-3 Hz) is achieved by the "EO+RS+ON" case. Most of the COIs show moderate spikes in the frequency range of 1-5 Hz, and are flat between 5-6.5 Hz. High-magnitude spikes indicate active stabilization effort to prevent instability, while moderate spikes mark the presence of some balancing strategy implemented by the PD patients.

The detailed linear fit parameters of each subset's mean IP curve are listed in Tables II and III. It is noticed that for the COIs, the slope is negative for all EO cases and positive for all but one EC case. This observation indicates that on the whole, for EC cases, there are more spikes at higher frequencies than other cases. The PD patients tried to stabilize their bodies by employing an ankle-like strategy to reduce their sway, which could be self-perceived as excessive. With the EO case, visual correction of perceived sway is possible, and few corrective measures are taken to allow for a more natural sway, which results in flat IP curves for PD patients. The absolute values of the slope are similar for COIs with the same visual and surface conditions, regardless of the medication state. The intercepts of the slopes, when arranged in ascending order, reveal pairs of COI subsets as: "EC+RS", "US+OFF", "EO+RS", and "US+ON". This suggests that balance in the RS test be heavily dependent on the visual feedback to the patients while the balance strategy for the US test is likely closely tethered to the medication intake.

Fig. 5(b) shows the IP frequency curve comparison among the PIGD and the TD GOIs. The average IP curve for subjects with PIGD shows a high amplitude of spikes at 2-4 Hz and high amplitude spikes for above 7 Hz. The TD IP curve on the other hand shows more spikes with moderate amplitude spread throughout all frequencies than other types of PD patients. For freezers, the absolute slope

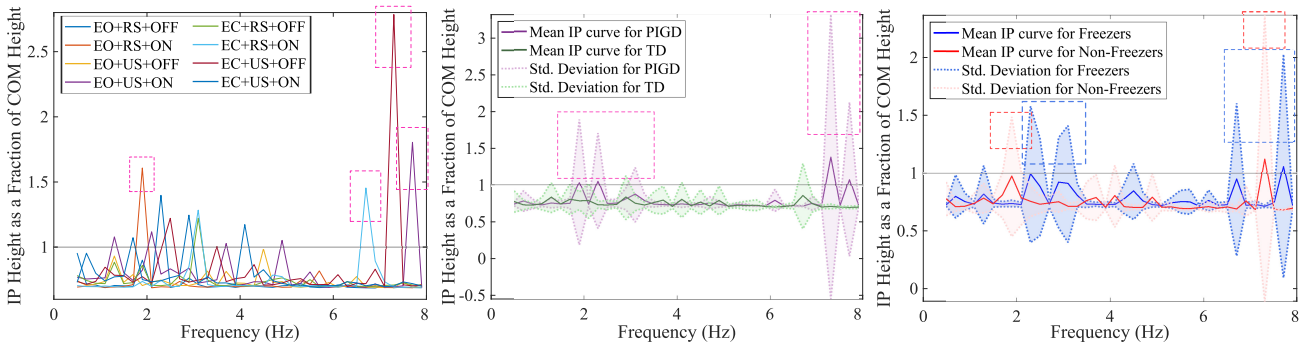

(a) (b) (c)

Fig. 5. IP height-frequency curves from experimental data: (a) Comparison among all COIs; (b) Comparison among PIGD and TD GOIs; (c) Comparison among freezers and non-freezers GOIs.

amplitude varies from the OFF to ON state, while there is not significant difference in non-freezers. This indicates that the medications have a pronounced effect on patients with FoG as expected. High-amplitude spikes in the mean IP curve are observed at ranges of 2-4 Hz and 6-8 Hz in freezers and 1.5-2.5 Hz and 7-7.5 Hz in non-freezers; see Fig. 5(c). Across all GOIs, it is noticed that the slopes of the linear fits are almost flat for the case of "EC+RS+OFF". It was found that the phenomenon was due to spikes at all frequencies and this implies that there was no structured balance strategy except undirected efforts to stabilize upright gait.

C. Model Simulation Results

To statistically analyze the IP curves, a one-way ANOVA was employed to extract the mean and standard deviation of IP curves across various subgroups. Specifically, the focus of COI was on the "EO+RS+OFF" condition as the TIP model considered is relatively simple with a stable base. The simulated IP curves were obtained from the LQR-controlled TIP model. In order to find the best-fit model parameters for each GOI's mean IP curve, the linear fits for the several simulated IP curve sets were found. Each experimental IP curve's linear fit was compared against the simulated IP curve linear fits; see Fig. 6. The average error between the linear fits was computed as

$$e = \sum_{i=1}^{N} \frac{|\text{fit}^{exp}(i) - \text{fit}^{sim}(i)|}{N}, \tag{6}$$

where N is the number of frequency bands under consideration, $\text{fit}^{exp}(i)$ and $\text{fit}^{sim}(i)$ are the mean GOI and the simulated IP curves for the ith frequency band, respectively. The model parameter set for which magnitude of e was minimized with respect to a given GOI was considered the best-fit parameter set for that GOI.

The best-fit model parameters that were able to describe the "EO+RS+OFF" experimental IP curves were highly dissimilar from those of healthy IP curves; see Table IV. For example, α for normal IP curves is around 10^6, implying that healthy subjects use a minimum effort control strategy to balance [14]. However, in the abnormal PD experimental

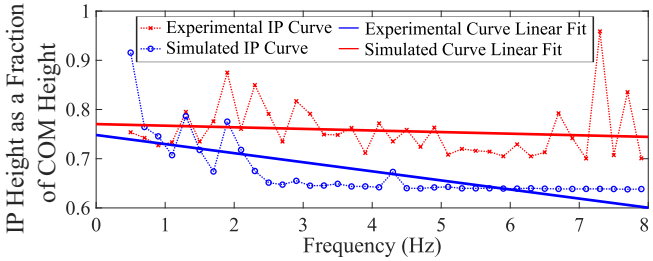

Fig. 6. Example of finding the experimental and simulated IP curve linear fits for comparison.

TABLE IV

THE LQR CONTROLLER PARAMETERS FOR VARIOUS CASE STUDIES

S	Case	α	β_1	β_2	β_3	σ_1	σ_2	σ_3
1	Overall	10	1	0.1	0.1	0	1	1
2	PIGD	10	1	0.1	1	0	1	1
3	TD	10	1	0.1	0.1	0	1	0
4	Freezer	10	1	0.1	1	0	0	1
5	Non-Freezer	10	1	0.1	0.1	0	1	1

IP curves, the number of parameter sets increases as α goes below a magnitude of 10. This indicates that the control strategy employed by PD patients requires considerable effort. Several combinations of the $\boldsymbol{\beta}$ and $\boldsymbol{\sigma}$ parameters were examined. It was found that ankle effort was more heavily penalized than knee and hip effort, contrary to the usual heavy penalization of hip strategy [14]. It was also found that knee actuation cannot be penalized heavily to get the experimental IP curve behavior. This indicates that the patients heavily use knee and hip strategies to balance compared to healthy subjects. The best-match relative noise was found when less number of joint strategies were involved, that is, when the $\boldsymbol{\sigma}$ set had not more than two non-zero elements.

On comparing the best-fit parameters of each GOI with the overall parameters describing the experimental PD dataset, we observed the differences in the balance preferences of each subgroup. The PIGD phenotype and freezers penalized hip strategy as much as they penalized ankle strategy. The TD phenotype engaged fewer joints to balance than other types of PD patients. Similarly, freezers used less joints than non-freezers in their balance strategy. The use of knee joint

strategy was preferred across all the cases.

IV. Discussion

Our findings reveal that the extracted PD patients' IP curves do not match all three typical characterization patterns seen in healthy individuals. While further investigations are needed to validate the efficacy of IP curves in distinguishing PD patients from healthy subjects, they hold substantial promise as a gait-based diagnosis method for PD. Despite limitations to the "EO+RS+OFF" case, an advanced comprehensive model could systematically analyze PD patient gait across various test scenarios.

The flatness observed in PD IP curves may indicate a lack of sophisticated balance strategies in PD patients. The work in [14] eliminated a single-inverted pendulum (SIP) model approach to replicate the IP phenomena of healthy humans at quiet stance. Similar to the PD IP curves in this work, the SIP model cannot produce the IP curve characterization patterns. However, unlike the SIP IP curves, which cannot exceed COM mathematically, PD IP curves exhibit spikes surpassing the COM. The observed spikes vary in amplitudes from mild to extreme and range from none to numerous. These spikes suggest that PD patients attempt to employ ankle strategies to stabilize themselves. Nonetheless, this balancing strategy is non-optimal and can potentially contribute to balance instability.

The IP method was able to provide insights into the preferred neural balance strategy in PD subjects. The information it furnished is detailed and extensive compared to other common frequency analysis methodologies (e.g., power spectral density) and balance metrics (e.g., COP and COM excursions [24]). While the IP curves themselves can act as a diagnostic tools, the LQR-controlled TIP model offers an avenue to further assess existing underlying neuromuscular behavior and control strategies at the joint level. Gaining in-depth understanding into quantifiable differences in gait characteristics among PD phenotypes is essential to develop custom rehabilitation strategies and to design assistive exoskeleton controllers to specifically target the motor movement deficiencies and balance challenges.

V. Conclusion

This paper investigated frequency characteristics of quiet stance in PD patients. IP height analysis was performed on the patient data and the resultant curves were compared with IP curves generated from a LQR-controlled TIP model. The LQR parameters from the best linear fits were used to quantify neural balance strategies in PD patient subsets. Findings revealed significant differences in IP curve behavior between the PD patients and the healthy individuals. Future work includes applying advanced biomechanical models to other test cases and exploring IP frequency curves' potential as a diagnostic tool for PD.

References

[1] B. R. Bloem, M. S. Okun, and C. Klein, "Parkinson's disease," *The Lancet*, vol. 397, no. 10291, pp. 2284–2303, 2021.

[2] C. D. Marsden, "Parkinson's disease." *J. Neurology, Neurosurg., Psych.*, vol. 57, no. 6, p. 672, 1994.

[3] E. Tolosa, G. Wenning, and W. Poewe, "The diagnosis of parkinson's disease," *Lancet Neurol.*, vol. 5, no. 1, pp. 75–86, 2006.

[4] D. Heisters, "Parkinson's: symptoms, treatments and research," *British J. Nursing*, vol. 20, no. 9, pp. 548–554, 2011.

[5] M. Romanato, F. Spolaor, C. Beretta, F. Fichera, A. Bertoldo, D. Volpe, and Z. Sawacha, "Quantitative assessment of training effects using eksogt® exoskeleton in parkinson's disease patients: A randomized single blind clinical trial," *Contemp. Clin. Trials*, vol. 28, p. 100926, 2022.

[6] A. Ortlieb, M. Bouri, R. Baud, and H. Bleuler, "An assistive lower limb exoskeleton for people with neurological gait disorders," in *Proc. IEEE Int. Conf. Rehab. Robot.*, London, UK, 2017, pp. 441–446.

[7] J. Yi, D. Soudbakhsh, Y. Zhang, and Y. Zhang, "Why some Parkinson's disease patients cannot stand or walk but can ride a bicycle – A control system-based analysis," in *Proc. ASME Dyn. Syst. Control Conf.*, Ft. Lauderdale, FL, 2012, article # DSCC2012-8735.

[8] K. Low, "Robot-assisted gait rehabilitation: From exoskeletons to gait systems," in *2011 Defense Sci. Res. Conf. Expo*, Singapore, 2011, pp. 1–10.

[9] C. Zhu and J. Yi, "Knee Exoskeleton-Enabled Balance Control of Human Walking Gait with Novel Foot Slip," *IEEE Robot. Automat. Lett.*, vol. 8, no. 11, pp. 7751–7758, 2023.

[10] S. Rezvanian, T. Lockhart, C. Frames, R. Soangra, and A. Lieberman, "Motor subtypes of parkinson's disease can be identified by frequency component of postural stability," *Sensors*, vol. 18, no. 4, p. 1102, 2018.

[11] S. Kim, F. B. Horak, P. Carlson-Kuhta, and S. Park, "Postural feedback scaling deficits in Parkinson's disease," *J. Neurophysiol.*, vol. 102, pp. 2910–2920, 2009.

[12] P. Gorzelic, S. Schiff, and A. Sinha, "Model-based rational feedback controller design for closed-loop deep brain stimulation of parkinson's disease," *J. Neural Eng.*, vol. 10, no. 2, p. 026016, 2013.

[13] W. L. Boehm, K. M. Nichols, and K. G. Gruben, "Frequency-dependent contributions of sagittal-plane foot force to upright human standing," *J. Biomech.*, vol. 83, pp. 305–309, 2019.

[14] K. Shiozawa, J. Lee, M. Russo, D. Sternad, and N. Hogan, "Frequency-dependent force direction elucidates neural control of balance," *J. Neuroeng. Rehabil.*, vol. 18, no. 1, pp. 1–12, 2021.

[15] M. Günther, S. Grimmer, T. Siebert, and R. Blickhan, "All leg joints contribute to quiet human stance: a mechanical analysis," *J. Biomech.*, vol. 42, no. 16, pp. 2739–2746, 2009.

[16] A. Yamamoto, S. Sasagawa, N. Oba, and K. Nakazawa, "Behavioral effect of knee joint motion on body's center of mass during human quiet standing," *Gait Posture*, vol. 41, pp. 291–294, 2015.

[17] G. Sreenivasan, C. Zhu, and J. Yi, "Neural balance control of human quiet stance for construction workers," in *Proc. IEEE Conf. Automat. Sci. Eng.*, Auckland, New Zealand, 2023, pp. 1–6.

[18] K. G. Gruben and W. L. Boehm, "Force direction pattern stabilizes sagittal plane mechanics of human walking," *Hum. Movement Sci.*, vol. 31, no. 3, pp. 649–659, 2012.

[19] M. A. Sharbafi, C. Maufroy, M. N. Ahmadabadi, M. J. Yazdanpanah, and A. Seyfarth, "Robust hopping based on virtual pendulum posture control," *Bioinsp. Biomim.*, vol. 8, no. 3, p. 036002, 2013.

[20] G. Sreenivasan, C. Zhu, and J. Yi, "Knee stiffness in assistive device control at quiet stance: A preliminary study," *IFAC PapersOnLine*, vol. 56, no. 3, pp. 163–168, 2023.

[21] K. G. Gruben and W. L. Boehm, "Mechanical interaction of center of pressure and force direction in the upright human," *J. Biomech.*, vol. 45, no. 9, pp. 1661–1665, 2012.

[22] C. E. N. de Oliveira, C. Ribeiro de Souza, R. d. C. Treza, S. M. Hondo, C. Bernardo, T. K. F. Shida, L. Dos Santos de Oliveira, T. M. Novaes, D. d. S. F. de Campos, E. Gisoldi *et al.*, "A public data set with ground reaction forces of human balance in individuals with parkinson's disease," *Front. Neurology*, vol. 16, p. 865882, 2022.

[23] M. Prime, J. L. McKay, A. Bay, A. Hart, C. Kim, A. Abraham, and M. E. Hackney, "Differentiating parkinson disease subtypes using clinical balance measures," *J. Neurol. Phys. Ther.*, vol. 44, no. 1, p. 34, 2020.

[24] S. Chen, Y. Yu, C. Di, M. Trkov, J. Gong, and J. Yi, "Postural balance of kneeling gaits on inclined and elevated surface for construction workers," in *Proc. IEEE Conf. Automat. Sci. Eng.*, Lyon, France, 2021, pp. 753–758.